DE GRUYTER DOI 10.1515/zpch-2014-0002 — Z. Phys. Chem. 2014; 228(4–5): 521–541

Mark T. Greiner*, Tulio C. R. Rocha, Benjamin Johnson, Alexander Klyushin, Axel Knop-Gericke, and Robert Schlögl

The Oxidation of Rhenium and Identification of Rhenium Oxides During Catalytic Partial Oxidation of Ethylene: An In-Situ XPS Study

Abstract: Rhenium is catalytically active for many valuable chemical reactions, and consequently has been the subject of scientific investigation for several decades. However, little is known about the chemical identity of the species present on rhenium surfaces during catalytic reactions because techniques for investigating catalyst surfaces in-situ – such as near-ambient-pressure X-ray photoemission spectroscopy (NAP-XPS) – have only recently become available. In the current work, we present an in-situ XPS study of rhenium catalysts. We examine the oxidized rhenium species that form on a metallic rhenium foil in an oxidizing atmosphere, a reducing atmosphere, and during a model catalytic reaction (i.e. the partial-oxidation of ethylene).

We find that, in an oxidizing environment, a Re_2O_7 film forms on the metal surface, with buried layers of sub-oxides that contain Re^{4+}, Re^{2+} and $Re^{\delta+}$ ($\delta \sim 1$) species at the Re_2O_7/Re interface. The Re^{2+} containing sub-oxide is not a known bulk oxide, and is only known to exist on rhenium-metal surfaces. The Re_2O_7 film sublimes at a very low temperature (*ca.* 150 °C), while the Re^{4+}, Re^{2+} and $Re^{\delta+}$ species remain stable in oxidizing conditions up to at least 450 °C. In a reducing atmosphere of H_2, the Re^{2+} species remain on the surface up to a temperature of 330 °C, while $Re^{\delta+}$ species can be detected even at 550 °C.

Under conditions for partial-oxidation of ethylene, we find that the active rhenium catalyst surface contains no bulk-stable oxides, but consists of mainly Re^{2+} species and small amounts of Re^{4+} species. When the catalyst is cooled and inactive, Re_2O_7 is found to form on the surface. These results suggest that Re^{2+} and Re^{4+} species may be active species in heterogeneous rhenium catalysts.

Keywords: Near-Ambient Pressure Photoemission Spectroscopy, Rhenium Oxide, Rhenium Oxidation, Ethylene Epoxidation, Rhenium Catalyt.

***Corresponding Author: Mark T. Greiner,** Fritz-Haber Institut der Max-Planck Gesellschaft, Department of Inorganic Chemistry, 4–6 Faradayweg, 14195, Berlin, Germany, e-mail: mgreiner@fhi-berlin.mpg.de

Tulio C. R. Rocha, Benjamin Johnson, Alexander Klyushin, Axel Knop-Gericke, Robert Schlögl: Fritz-Haber Institut der Max-Planck Gesellschaft, Department of Inorganic Chemistry, 4–6 Faradayweg, 14195, Berlin, Germany

Dedicated to: Professor Klaus Rademann on the occasion of his 60th birthday

1 Introduction

Rhenium is used as a catalyst for major industrial chemical processes. Its main application is in the petroleum industry, where it is alloyed with Pt and used for catalytic reformation of napthas into high-octane hydrocarbons. [1–5] This application has led to research on rhenium's role in the cracking and de-hydrocondensation of alkanes. [6–8] Rhenium is also heavily utilized – in the form of Re_2O_7 on Al_2O_3 supports – as a catalyst for olefin metathesis. [1, 9] On a smaller research scale, rhenium has been used as a promoter for cobalt catalysts in Fischer-Tropsch synthesis, [10] as a catalyst (alloyed with Pt) for the conversion of glycerol to syngas, [11] to catalyze selective oxidation of methanol and ethanol into aldehydes, [12–14] to catalyze selective hydrogenation of amides, [15] for N_2 dissociation in ammonia synthesis, [16, 17] and as a promoter for silver catalysts in ethylene epoxidation. [18]

The motivation of the present research is focused on rhenium's use as a promoter for partial-oxidation reactions. It has been shown previously that the addition of rhenium to silver catalysts can enhance the selectivity for production of ethylene epoxide, [18] but little is known about the chemical origin of the enhancement. In order to understand rhenium's behavior in bi-metallic partial-oxidation catalysts, and furthermore, to understand the complex rhenium-oxide/support interactions in working catalysts, [19] and the oxidation/reduction pretreatments often implemented for supported rhenium catalysts, [20] it is important to clearly understand the oxidation and reduction behavior of pure metallic rhenium. However, studies on the oxidation behavior of rhenium metal, the growth of surface oxides and reduction of these oxides are relatively sparse (in comparison to metals like iron or aluminum).

Given the large number of oxidation states that rhenium exhibits, its oxidation behavior is expected to be rather complex. The stable binary oxides of rhenium are ReO_2, ReO_3 and Re_2O_7, containing rhenium in the +4, +6 and +7 oxidation states, respectively. [21, 22] The Re^{6+} cation in ReO_3 is not especially stable, and disproportionates to Re^{7+} and Re^{4+} upon heating above 400 °C. [21, 22] ReO_2 is stable against disproportionation up to 850 °C. [22] Re_2O_7 is chemically

stable, but sublimes at a relatively low temperature (reported to be between 225–315 °C). [22–24] The existence of a Re^{5+} species in binary oxides is inconclusive; however, in rhenium-oxide bronzes (e.g. rhenium oxides alloyed other cationic elements), rhenium oxidation states of +4, 5, 6 and 7 are all possible. [25] Re^{3+}, Re^{2+} and Re^{1+} are not known to exist as oxides, but have been reported in metal complexes – for example, using carbonyl or organo-metallic ligands. [21]

Rhenium has been the focus of catalysis research for several decades, and the oxidation states of rhenium catalysts have traditionally been determined using thermo-gravimetric titration measurements. [3, 19, 26–29] These methods yield stoichiometries indirectly, and often require one to speculate the surface species present in the working catalyst. Nonetheless, many valuable observations have come from such studies. For instance, it was found that rhenium oxides can exhibit strong support interactions (especially with Al_2O_3 supports), giving rise to unexpectedly high reduction and sublimation temperatures for Re_2O_7. [30]

The most direct means of identifying the chemical states of surface species is using electron spectroscopic methods, such as X-ray photoemission spectroscopy (XPS). Since the 1970s, many XPS studies have been performed to examine the chemical state of rhenium catalyst surfaces; however, due to instrumentation limitations, these studies were performed ex-situ. [14, 20, 23, 31–35] The problem with ex-situ studies is that the rhenium oxidation states that are measured post-reaction can differ substantially from the species that are present in-situ.

Rhenium oxidation has been investigated by several groups using ultra-high-vacuum (UHV) surface science techniques, in which rhenium single crystals of several orientations have been examined after various O_2 exposures and temperature treatments. [13, 36–41] These studies have provided a thorough understanding of the rhenium metal surface during the onset of oxidation. High-resolution photoemission spectra have revealed well-resolved peaks that are associated with surface rhenium-oxygen bonds. Such spectra have resolved distinct photoemission peaks for rhenium surface atoms coordinated with one, two and three oxygen ions adsorbed to the surface. [38, 41]

One important question that arises from the UHV catalyst studies is whether such oxygen species can exist under reaction conditions (i.e. at higher pressures) – this question refers to the well-known 'pressure gap'. The recent development of Near-Ambient-Pressure XPS (NAP-XPS) has begun to fill the pressure gap. It is now possible to use XPS to analyze the surface species that are present during a catalytic reaction, in gas mixtures nearing ambient pressure.

In the present work, we have used NAP-XPS to examine, in-situ, the oxidation and reduction behavior of rhenium metal. We found that, when rhenium metal is oxidized at relatively low temperature (50 °C), a thin film of Re_2O_7 grows on the

metal surface. Using XPS depth profiling, we have characterized the structure of the rhenium oxide film, and found several intermediate rhenium oxidation states present at the interface between the Re_2O_7 film and the bulk rhenium metal – such as Re^{4+}, Re^{2+} and $Re^{\delta+}$, where $\delta \sim 1$. The Re^{4+} species are attributed to oxide-interface defects – rather than a distinct ReO_2 film – due to their low abundance. The Re^{2+} species are attributed to a surface oxide that in previous works has been attributed to 'ReO'. [13, 38] Although ReO is not known to exist as a bulk oxide, this species appears to be stable on rhenium metal surfaces. The $Re^{\delta+}$ species have been attributed to oxygen-reconstructed rhenium, in agreement with previous works. [13, 37–41]

We have also examined the thermal decomposition of the sub-nanometer-thick Re_2O_7 film and found that it begins to sublime at *ca.* 150 °C, a much lower temperature than has previously been reported for the bulk oxide. [22–24] It is also found that Re^{2+} species are stable on the metal surface, in an oxidizing environment, even at elevated temperatures (*ca.* 400 °C). We examined the reduction behavior of this oxidized surface species by heating samples in an H_2 atmosphere, and have found that the Re^{2+} species is stable in H_2 (P = 0.3 mbar) up to *ca.* 337 °C, while oxygen reconstruction species remain stable even up to 550 °C.

In order to examine the rhenium species that are present on an active catalyst, we have also examined rhenium in-situ, during the catalytic partial-oxidation of ethylene. While heating a rhenium foil sample in a gas atmosphere of O_2 and C_2H_4, we measured XPS spectra and simultaneously monitored the production of ethylene partial-oxidation products (C_2H_4O). It was found that when the catalyst is active (i.e. at a temperature of 350 °C), the surface exhibits only a thin layer of the Re^{2+} surface oxide ('ReO'), a small amount of Re^{4+} species – that were attributed to defects – and a buried layer of $Re^{\delta+}$ and Re^0. No stable bulk oxides (such as Re_2O_7, ReO_3 or ReO_2) were observed on the active catalyst surface. However, when the catalyst was inactive (i.e. at a lower temperature of 150 °C) the same species (Re^{2+}, Re^{4+}, $Re^{\delta+}$ and Re^0) were present, but a surface layer with Re_2O_7 was formed.

These findings suggest that Re^{2+} and Re^{4+} surface species may be responsible for the catalytic activity of rhenium during partial oxidation reactions, and that Re_2O_7 may inhibit partial-oxidation activity. The Re^{2+} species that we have observed here – although previously reported from UHV studies of rhenium oxidation – have not previously been identified as a species responsible for catalytic activity. Furthermore, as there is no known bulk Re^{2+} binary oxide, this oxidized species appears to be unique to rhenium metal surfaces/interfaces. Our results suggest that the Re^{2+} species may play a role in catalysis, and warrants a closer examination.

2 Experimental

Photoemission measurements were performed in a Near-Ambient-Pressure X-ray Photoemission Spectrometer (NAP-XPS) system, on the Innovative Station for In Situ Spectroscopy (ISISS) beamline at the Helmholz-Zentrum Berlin/BESSY II synchrotron facility. The experimental set-up has been described previously in detail. [42, 43] Briefly, the sample is housed in a chamber maintained at 0.3 mbar pressure of a reactant gas mixture. The pressure is maintained by the simultaneous operation of mass flow controllers – to control the in-flow of reaction gas mixtures – and a feed-back regulated valve between the chamber and a turbomolecular pump – to regulate the pumping speed.

The spectrometer utilizes a hemispherical analyzer that is operated in ultra-high vacuum. The pressure difference between the reaction cell and the analyzer is maintained using three differentially pumped stages. Each stage contains an electrostatic lens for gathering a wide-angle spread of photoelectrons and focusing the electrons onto the analyzer entrance slit. The position of the Fermi edge of the rhenium metal valence band was used for binding energy calibration. Spectra were measured using a pass energy of 10 eV, and photon energies ranging between 190 eV and 760 eV (depending on the desired escape depth). The total Gaussian resolution for the combination of photon source and spectrometer was 0.2 eV when using a photon energy of 190 eV and 0.4 eV when using a photon energy of 750 eV.

Samples are positioned within one millimeter of the first entrance aperture of the electrostatic lens system. Heating is accomplished with an infrared laser, which shines onto the back of the sample *via* a fiber-optic cable and infrared optics elements. Temperature is measured with a K-type thermoelement, that is held firmly to the top surface of the sample using a stainless steel mounting plate.

Samples were pre-cleaned by oxidation in 0.3 mbar of O_2 at 300 °C to remove surface carbon, followed by ion sputtering using 1 keV Ar^+ ions, to remove other surface contaminants that accumulated on the foils during handling (such as sodium, chlorine and silicon). Samples were then annealed in 0.3 mbar H_2 up to 550 °C to remove residual oxygen from the surface.

The surface oxide was grown by oxidizing a cleaned metallic foil in a mixture of O_2 and 1% O_3, at a total pressure of 0.3 mbar, and a temperature of 50 °C. The ozone was generated by flowing O_2 through an AC corona discharge ozone generator and into the analysis chamber though a leak valve.

Thermal decomposition of the oxide was performed with the sample in constant flow of the $O_2 + O_3$ mixture, while increasing the sample temperature in steps of 50 °C and simultaneously measuring XPS spectra once the sample

reaches steady state. Thermal reduction of the samples was accomplished similarly, but using a constant flow of H_2, at a total pressure of 0.3 mbar.

Ethylene partial oxidation was carried out by flowing a mixture of O_2 and C_2H_4 simultaneously into the chamber, using separate mass-flow controllers for each gas, to a total chamber pressure of 0.3 mbar. Several gas-feed ratios ($O_2 : C_2H_4$) ranging 1 : 100 and 2 : 1 were tested. In the gas reaction mixture, the sample temperature was ramped between 350 °C and 150 °C at a rate of 1.7 °C/min. Photoemission spectra were continuously measured throughout the temperature ramps.

During the temperature ramps, the production of partial oxidation products – having molecular formula C_2H_4O (i.e. ethene oxide and acetaldehyde) – were monitored using an on-line Proton-Transfer-Reaction Mass Spectrometer (PTRMS) by monitoring the ion with mass 45 amu (which represents the protonated $C_2H_4OH^+$ ion). Due to the vastly different proton affinities of C_2H_4O and CO_2, the PTRMS is not sensitive to CO_2. Therefore, the measured signal represents primarily the partial oxidation products of ethylene oxidation.

Rhenium foils were 99.95% purity, and purchased from American Elements. The rhenium oxide reference samples were powders, of 99.9+ % purity, purchased from Sigma-Aldrich, and were pressed into pellets.

The peak fitting of all spectra was accomplished using the software CasaXPS. The parameters used for fitting the high-resolution Re $4f$ spectra were determined as follows. The natural broadening of the Re $4f_{7/2}$ line is *ca.* 0.11 eV. [44] The expected total peak width was calculated according to Olivero and Longbothum [45] and yielded a value of 0.24 eV, which we used as the lower limit for the peak full-width-half-maximum (FWHM).

An asymmetric Doniach–Sunjic peak shape was used to fit the peaks for metallic rhenium, and for the peaks of the oxidized rhenium species that are expected to exhibit metallic behavior, [46] with an asymmetry parameter of 0.1 eV, consistent with previously reported Re $4f$ peak-fitting routines. [13, 39–41] The 7/2-5/2 spin-orbit coupling was set to be 2.42 eV for all peaks. The 7/2 : 5/2 peak area ratios were set to 4 : 3. The $4f_{5/2}$ peak was also set to have a FWHM 0.05 eV greater than the $4f_{7/2}$ peak, due to its shorter lifetime. [39]

The FWHM of the oxygen reconstruction peaks were set to be 0.05 eV larger than the metallic peak, and a more Gaussian-shape was allowed for these peaks in order to account for the likelihood that there are a multitude of reconstruction configurations on the polycrystalline foil with slightly different binding energies that those reported for single-crystal rhenium surfaces.

The higher oxidation states (+2, +4, +6 and +7) were allowed larger FWHM values. The Re^{7+} species had the largest FWHM value of 0.43 eV (for 190 eV photon energy) and the largest degree of Gaussian peak shape, which we attributed to the high degree of disorder and defects in the oxide.

The peak fitting parameters were first determined using the high-resolution spectra ($h\nu = 190$ eV, pass energy = 10 eV). The same peak parameters were then used to fit the lower resolution spectra ($h\nu = 750$ eV, pass energy = 10 eV), but 0.23 eV was added to the FWHM of each peak in order to account for the increased linewidth of the photon source at 750 eV.

3 Results and discussion

3.1 Rhenium oxide references

Before using photoemission to examine the oxidation properties of Re, it is important to first identify the Re $4f$ binding energies of the known rhenium oxides. The Re $4f$ spectrum can be difficult to analyze because at least six different oxidation states of rhenium can exist and their peak positions lay within a binding energy range of *ca.* 5–6 eV. Some oxidation states are separated from one another by as little as 0.2 eV. Furthermore, with the spin-orbit splitting of Re $4f$ of 2.42 eV, if a sample contains several oxidation states, Re $4f_{7/2}$ peak of a high oxidation state can overlap with the Re $4f_{5/2}$ peak of a low oxidation state, giving rise to a heavily convoluted XPS spectrum. Thus, reliable binding energy values are required to correctly identifying the rhenium species present.

However, there is somewhat large inconsistency in the reported Re $4f$ binding energies in the literature. For instance, the Re $4f_{7/2}$ binding energy of Re_2O_7 has been reported in the range of 45.4–46.9 eV. [20, 23, 29] Most of primary sources for binding energy values comes from a number of reports between the late 1970s and early 1990s. The most modern reliable primary source of data was reported by Somorjai *et al.*in 1988; [29] however, even this was measured using what is now dated equipment. Thus we find it appropriate to re-report the bulk rhenium oxide powder references for Re_2O_7, ReO_3, ReO_2 and reduced ReO_2 (i.e. ReO_2 annealed in vacuum to 450 °C) using a modern spectrometer and synchrotron radiation, as well as to establish an internally consistent set of Re $4f_{7/2}$ binding energies.

Figure 1a shows the Re $4f$ photoemission spectra of these oxides, along with peak fits and peak assignments. Note that the oxides tend to form a surface layer of Re_2O_7 when exposed to air, because Re_2O_7 is thermodynamically most stable. [21] Furthermore, Re_2O_7 is very hygroscopic, so this surface layer adsorbs water. [21] Thus the spectra of ReO_3 (Figure 1-ii) exhibits features from a *ca.* 2 nm-thick surface layer of Re_2O_7 and hydroxides, while ReO_2 (Figure 1-iii) is covered with a surface *ca.* 2 nm-thick layer of Re_2O_7 + ReO_3 + mixed hydroxides (depth profiles were determined from photon-dependant XPS measurements and are given in the sup-

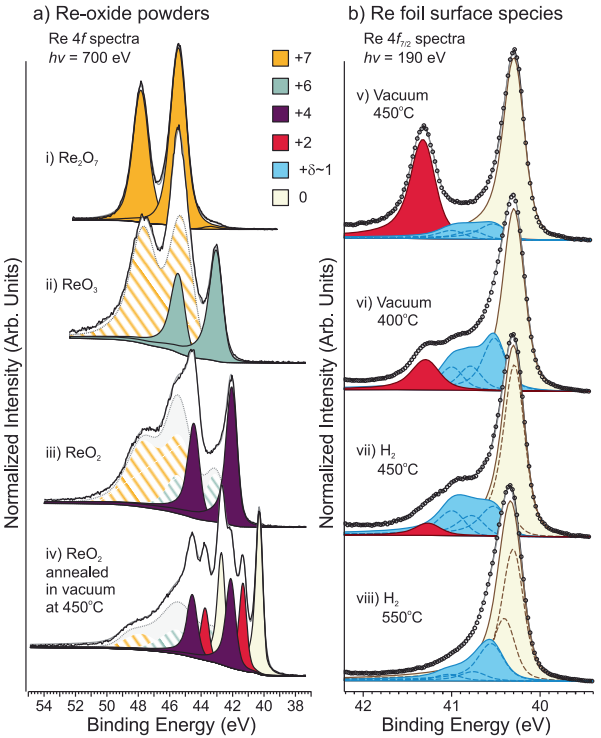

Figure 1: (a) Re 4f spectra of rhenium oxide reference compounds. The Re oxidation states are indicated in the legend. The hatched regions indicate ill-defined surface contaminants of 6+ and 7+ oxidation state, such as surface hydroxides. The black solid line represents the raw data, the grey solid line represents the sum of all synthetic peak fits, and dotted grey line represents the sum of the peak fits for the surface contaminants. A description of the peak fitting routine is given in the experimental section. (b) Re 4$f_{7/2}$ spectra of surface species that are found on Re metal foils. Empty circles represent raw data, the grey solid lines represent the sum of the peak fits. The dashed blue line indicates the peak fits used for the oxygen-reconstructed rhenium species. The dashed brown line indicates the peak fits used to fit the metallic peak caused by the surface core-level shift (note that it is only significant in the spectrum at 550 °C). The peak fitting routine is described in the experimental section.

plementary information). These surface contaminants give rise to broad, poorly-resolved features towards the high-binding-energy end of the spectra, as indicated in Figure 1a by the hatched regions. These surface layers were not removed prior to spectra collection (i.e. *via* heating or sputtering) so as not to disrupt the underlying stoichiometric oxide. The surface contaminants were fit using broadened Gaussian-shaped peaks, with one set of spin-orbit-split peaks for the Re^{7+} species and one set of spin-orbit-split peaks for the Re^{6+} species. The spin-orbit splitting

Table 1: Compilation of Re $4f_{7/2}$ binding energies, chemical shifts relative to Re^0, and the assigned Re oxidation state and Re species associated with each binding energy. Note that the values for δ^1, δ^2 and δ^3 species are taken from literature values, [39] while the values for the oxidation states 0, 2, 4, 6 and 7 were measured in this study. The species denoted by $Re\text{-}O_{(x)}$ represent rhenium metal surface atoms coordinated with 1–3 oxygen ions. Also note that the species denoted 'ReO' actually has an unknown stoichiometry. Uncertainty in the binding energy for Re^0 is *ca.* ±0.02 eV. The Re^{2+} species can shift by ±0.05 eV depending on other neighboring species. Uncertainty in the Re^{4+} and Re^{6+} species are ±0.05. The Re^{7+} binding energy can shift by *ca.* 0.2 eV, because it is a semiconductor and the position of it Fermi level is sensitive to the presence of defects. [47, 48]

Oxidation state	B.E. (eV)	Chemical Shift	Species
0	40.35	0	Metal
δ^1 (~ 1)	40.57†	+0.22	$Re\text{-}O_{(1)}$
δ^2 (~ 1)	40.84†	+0.49	$Re\text{-}O_{(2)}$
δ^3 (~ 1)	41.08†	+0.73	$Re\text{-}O_{(3)}$
2	41.45	+1.10	'ReO'
4	42.20	+1.6	ReO_2
6	43.10	+2.8	ReO_3
7	45.5	+5.1–5.3	Re_2O_7

† Values taken from references. [38, 39]

was held constant at 2.42 eV for these peaks, and the 7/2:5/2 ratio was held at 4 : 3. Despite the surface contamination features in the XPS spectra, the Re^{6+} peak of the ReO_3 reference sample and Re^{4+} peak of ReO_2 reference sample are well resolved and give rise to reliable binding energies.

A number of additional peaks can be generated upon heating ReO_2 in vacuum. During annealing in vacuum (450 °C) the oxide becomes reduced, giving rise to a mixture of oxidation states, including Re^{2+} and Re^0, as shown in Figure 1-iv. Note that ReO is not a known bulk oxide, but has only been observed at the interface to Re metal. [13, 38] The simultaneous presence of Re^{2+} and Re^0 in this spectrum is consistent with these previous observations. By fitting the spectra, using appropriate restrictions (such as a spin-orbit splitting of 2.42 eV, and a $4f_{7/2} : 4f_{5/2}$ ratio of 4 : 3) we were able to identify the binding energies of the Re^{7+}, Re^{6+} and Re^{4+} states in the respective oxides. These values are given in Table 1.

3.2 Surface oxides on rhenium metal

In addition to the known bulk oxides, various oxidized Re species are known to form on Re metal surfaces. Figure 1b shows a selection of Re $4f_{7/2}$ photoemis-

sion spectra of rhenium foils under various conditions, to demonstrate the surface species that are possible. These species include various O-terminations of Re (i.e. Re surface atoms bonded to various numbers of oxygen ions). [38, 39, 41] The surface coordination of Re with oxygen gives rise to distinct shoulders on the high-binding-energy side of the metallic peak in the Re 4*f* XPS spectra, as shown in Figure 1b. Three distinct peaks have been reported in the literature, in which Re is coordinated with 1, 2 or 3 oxygen anions. [38, 39, 41] These Re atoms have formal charge of *ca.* +1. As seen in Figure 1b, the populations of these species can change depending on the conditions.

The first 'oxide' to form is 'ReO', having the formal oxidation state of +2. Based on available literature, ReO does not exist as a bulk oxide. [21] There is no reported crystal structure of this species; however, 'ReO' has been observed on several accounts *via* XPS measurements, in studies of oxidized rhenium metal surfaces. [13, 29, 38, 40] The 'ReO' (or Re^{2+}) species gives rise to a distinct peak in the Re 4*f* photoemission spectrum, at a $4f_{7/2}$ binding energy of *ca.* 41.45 eV, as shown in Figure 1b. We will continue throughout this report to refer to this species as 'ReO'; however, we do not commit to the notion that the stoichiometry of this species is actually ReO. Further structural studies are needed to understand this species more thoroughly.

In addition to the unique 'ReO' and O-coordinated Re surface species, under certain conditions (discussed further below with Figure 4) a small intensity of an additional species can be observed as a shoulder on the high-binding-energy side of the 'ReO' 4*f* peak. This feature is illustrated in Figure 2. Given that its binding energy of 41.9 eV is similar to that of ReO_2, we attribute this species to an Re^{4+} state. A similar state has been observed previously, and attributed to Re_2O_3 (i.e. Re^{3+}); [13] however, Re_2O_3 is not a known oxide, and Re^{3+} is not known to exist as a stable oxide species. [21, 25] Therefore we believe it is more likely that this species is from Re^{4+}.

The 'ReO' and O-coordinated Re species are thermally stable. They exist at relatively high temperatures even in H_2. However at lower temperatures, other Re oxides are stable. Figure 3 shows Re 4*f* photoemission spectra of Re foil oxidized in a mixture of O_2 + 1% O_3 (P_{total} = 0.3 mbar), oxidized at 50 °C. Here one can see that a film of Re_2O_7 grows on the outer layer of the surface oxide. It is interesting to note the absence of Re^{6+} and the minute amount of Re^{4+}. It is known from other metal/metal-oxide interfaces that the metal oxidation state increases progressively through the oxide film, going from the metal to the highest oxide. For example, iron oxides grow as Fe → FeO → Fe_3O_4 → Fe_2O_3, with Fe oxidation state of 0 → +2 → +2/+3 → +3. [49–52] In the case of Re, one might expect that the Re oxidation state in an oxide film should proceed as 0 → +1 → +2 → +4 → +6 → +7, however, here we see there is no Re^{6+} and only a small amount of Re^{4+}.

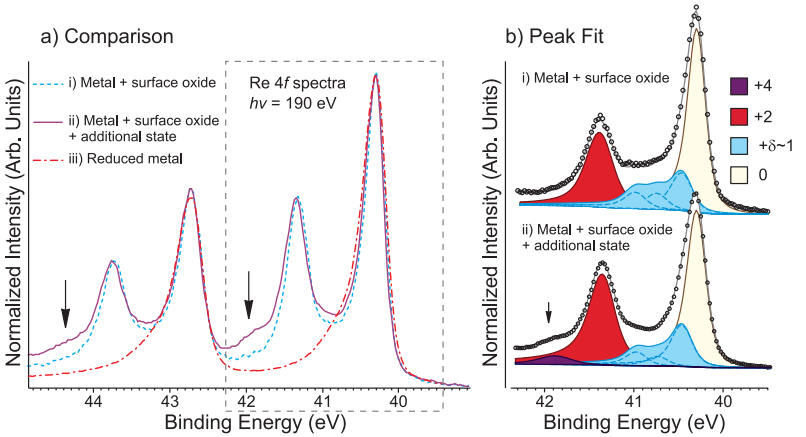

Figure 2: (a) Re 4f spectra of oxidized surface species on rhenium foil. Arrows point to a shoulder that is believed to be caused by Re^{4+} species. Spectrum i) shows the metal with a thin surface oxide, and was measured in vacuum (10^{-6} mbar) at 450 °C. Spectrum ii) shows the metal with a thin surface oxide with an additional Re chemical state, and was measured in 0.3 mbar of a gas mixture of 2 : 1, $O_2 : C_2H_4$ at 350 °C. Spectrum iii) shows the reduced metal, and was measured in 0.3 mbar of H_2 at 550 °C. (b) Re $4f_{7/2}$ spectra, with corresponding peak-fits from spectra i) and ii). The arrow points to a shoulder on the Re^{2+} peak. We attribute this shoulder to a minority species from Re^{4+} defects. Empty circles represent raw data, the grey solid lines represent the sum of the peak fits.

3.3 Structure of the surface oxide

In order to further understand the structure of the oxide, a depth profile was performed by tuning the photon energy. The XPS spectra of the oxide film were measured using a photon energy of 190 eV for the surface-sensitive spectrum, and a photon energy of 750 eV for the bulk-sensitive spectrum. These photon energies give rise to electron kinetic energies of *ca.* 150 eV and 710 eV, respectively, with corresponding inelastic mean-free-paths in Re_2O_7 of 0.56 nm and 1.42 nm, respectively. [53] The Re 4f spectra are shown in Figure 3, along with the corresponding peak fits. It should be noted that the bandwidth of the excitation source at 750 eV is significantly broader than the bandwidth of the excitation source at 190 eV. Consequently, the bulk-sensitive spectrum has a lower resolution than the surface-sensitive spectrum.

In order to obtain a reliable peak fit to the low-resolution, bulk-sensitive spectrum, we first fit the high-resolution spectrum. Then, using the peak shape and peak position parameters from the high-resolution spectrum, and increasing the full-width-half-maximum parameters of all peaks by a constant amount

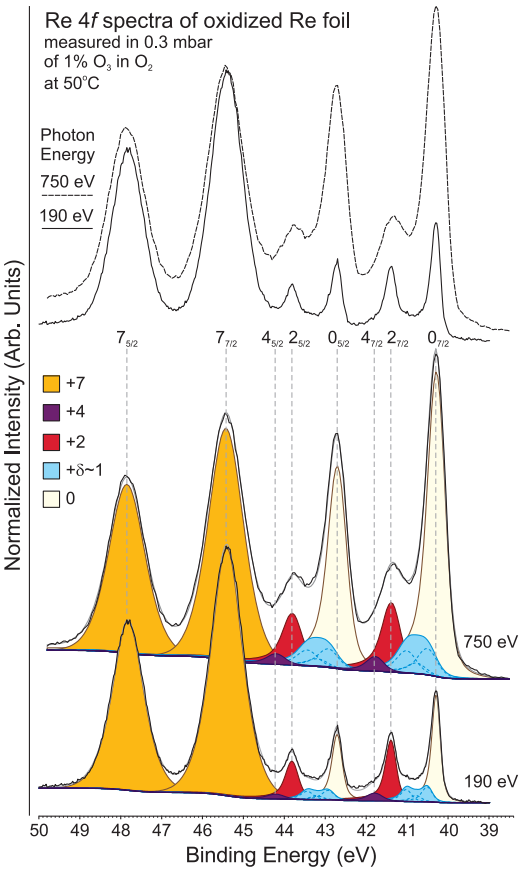

Figure 3: Re 4*f* spectra of rhenium foil oxidized in 0.3 mbar mixture of 99%O_2 and 1%O_3 at 50 °C. The top spectra show a comparison of the spectra measured with a surface-sensitive photon energy ($h\nu = 190$ eV) and a sub-surface sensitive photon energy ($h\nu = 750$ eV). The peak assignments are indicated using dashed grey lines. The two lower spectra show the peak fits for the two upper spectra. The peak areas from these fits were used to calculate the oxide film thickness.

of 0.23 eV, we fit the low-resolution spectrum by only allowing the variation in the peak area. Note that the relative peak areas of the three O-reconstruction peaks were kept constant to avoid arbitrary area changes of the individual O-reconstruction peaks. This is a reasonable restriction given that all the O-reconstruction peaks originate from approximately the same depth.

The proposed layered structure of the oxide film is presented in Figure 4. By comparing relative peak areas from the bulk- and surface-sensitive spectra, the order of the oxide layers was determined to be Re_2O_7, 'ReO', Re-O_x, Re, with Re_2O_7

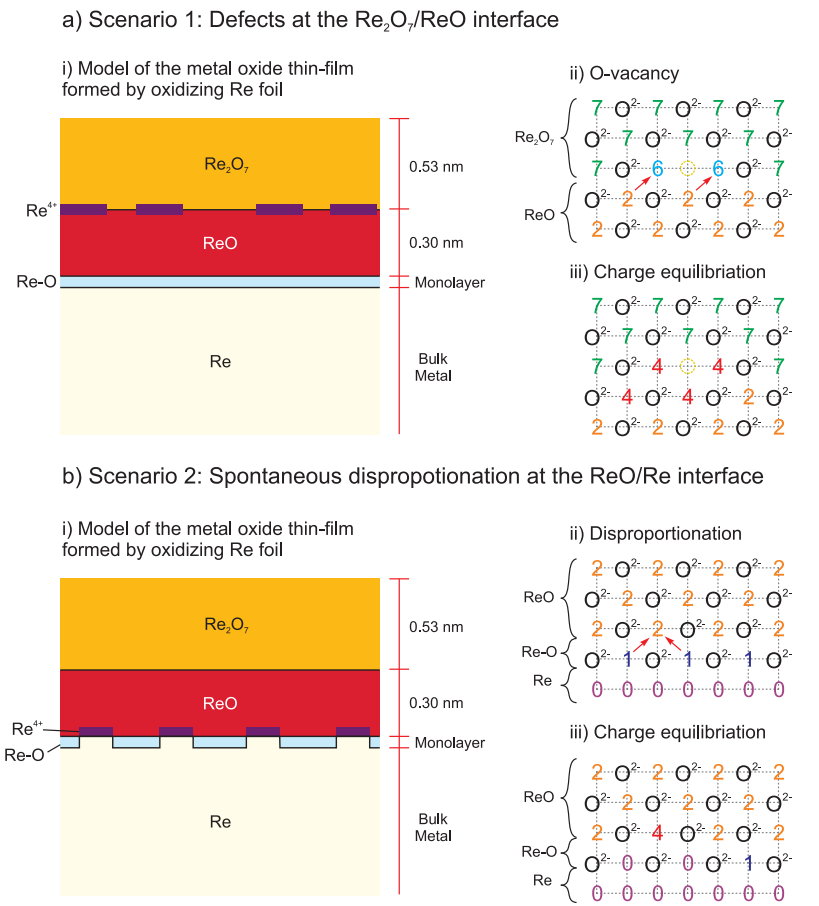

Figure 4: Schematic models of the proposed rhenium oxide film structure. Based on the photon-dependent depth profile data, shown in Figure 3, we determined that the film consists of an over-layer of Re_2O_7, an interlayer of an Re^{2+} species ('ReO'), an inter-layer of oxygen-reconstructed metallic rhenium, and the buried rhenium metal substrate. Re^{4+} species are also identified. We have identified two possible scenarios for the formation of Re^{4+}, as shown in (a) and (b). In the first scenario, Re^{4+} is caused by interfacial O-vacancies, and forms at the Re_2O_7/ReO interface. In the second scenario, Re^{4+} forms by disproportionation of Re^{1+} species, and resides at the ReO/Re interface. The colored numbers in the diagram refer to the oxidation state of rhenium.

being the outermost layer and Re being the buried bulk metal. Note that Re-O_x denotes the oxygen-reconstruction layer. Based on the measured peak areas (and following calculations presented in the supplementary information) the oxide consists of a *ca.* 0.53 nm thick layer of Re_2O_7, on top of a *ca.* 0.3 nm layer of 'ReO'.

The Re^{4+} species is found to be too low in concentration to be considered as a distinct layer, so we propose that it is a defect species. Based on the peak area analysis, the Re^{4+} signal appears to originate from between the 'ReO' and the Re-O_x layers, as illustrated in Figure 4b. However, due to the error involved in fitting the low-resolution, bulk-sensitive spectrum, it is also possible that the Re^{4+} signal actually originates from between the Re_2O_7 and 'ReO', as illustrated in Figure 4a.

We can propose two possible origins to the formation of Re^{4+} species. If the species exists at the Re_2O_7/'ReO' interface (scenario 1) then it could be that oxygen vacancy defects at the Re_2O_7/'ReO' interface give rise to the Re^{4+} species. In this scenario, one O^{2-} vacancy would give rise to two Re^{6+} centers. Oxygen vacancies at the Re_2O_7/'ReO' interface would allow for two Re^{2+} ions to transfer charge to two Re^{6+} ions, giving rise to four Re^{4+} ions per O-vacancy. This scenario is illustrated in Figure 4a-ii and -iii. This scenario appears plausible, when one considers the wealth of structural information known from studies on the structures of rhenium oxide bronzes. It is known that bronzes containing the Re in oxidation states of < +6 can lead to the formation of clusters containing Re^{4+} species and Re-Re bonds. [21] The formation of such bonds could be the driving force for the formation of Re^{4+} species from Re^{6+} species.

An alternative explanation to the presence of these Re^{4+} species is illustrated in Figure 4b-ii and -iii (scenario 2). In this scenario, the Re^{4+} species are formed at the 'ReO'/Re-O_x interface. They would form by spontaneous disproportionation of Re^{1+} species, in which two Re^{1+} ions (from the O-reconstruction layer) transfer electrons to one Re^{2+} ion (in the 'ReO' layer), resulting in one Re^{4+} ion and two Re^0 atoms. In fact the annealed ReO_2 reference, presented in Figure 1-iv, demonstrates the coexistence of Re^{4+}, Re^{2+} and Re^0 species. The fact that decomposition of ReO_2 led to a mixture of Re^{4+}, Re^{2+} and Re^0 species indicates that the energy barriers for electron transfer reactions between Re^0, Re^{2+} and Re^{4+} have relatively similar magnitudes.

Given that catalytic reactions are often carried out at elevated temperatures (*ca.* 200–400 °C), we examined the thermal stability of the oxidized species on the foil surface in oxidizing and reducing environments. Figure 5a shows a series of Re 4*f* spectra for a rhenium foil being heated in a mixture of O_2 + 1% O_3 (total pressure of 0.3 mbar), and Figure 5b shows the Re $4f_{7/2}$ region of a rhenium foil heated in H_2 (total pressure of 0.3 mbar).

The sample in Figure 5a, consists of a thin Re_2O_7 film at low temperature (50 °C), as well as photoemission features from the underlying 'ReO' layer and Re metal. At the moderately low temperature of 150 °C, the Re_2O_7 signal begins to decrease, indicating the onset of sublimation of Re_2O_7. This oxide is known to be volatile; however, the sublimation temperature is often quoted to be around

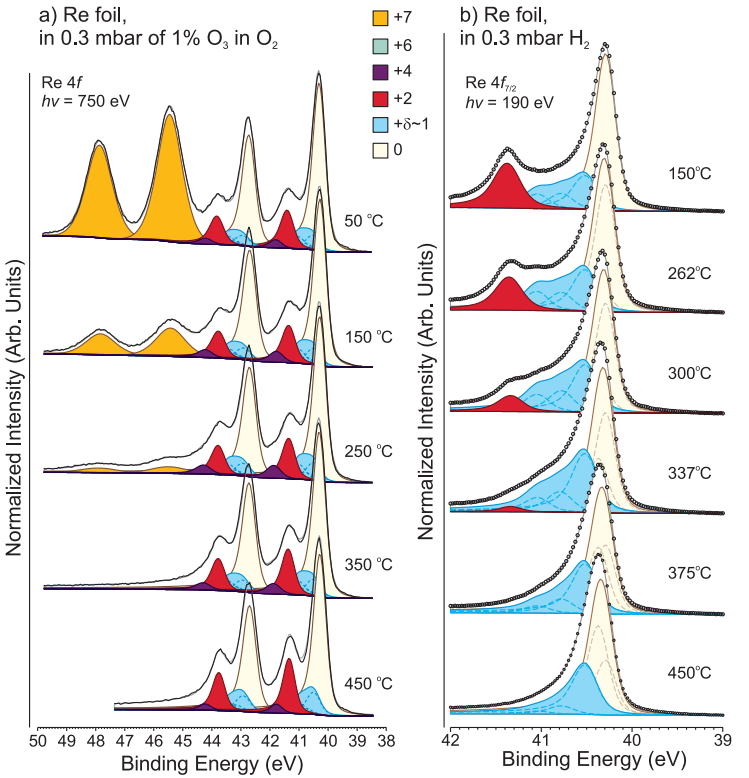

Figure 5: (a) Re $4f$ spectra, along with peak fits, of an oxidized rhenium foil being heated in a 0.3 mbar mixture of 99%O_2 and 1%O_3. (b) Re $4f_{7/2}$ spectra, along with peak fits, of a rhenium foil with oxidized surface species (Re^{2+} and $Re^{\delta+}$) being heated in 0.3 mbar of H_2. Rhenium oxidation states are indicated by the legend. Dashed brown lines indicate the surface and bulk metallic peaks used to fit the rhenium metal spectrum. Dashed blue lines indicate the peaks used to fit the oxygen-reconstruction species.

300 °C. Here we can see that Re_2O_7 sublimation begins at a considerably lower temperature. The discrepancy is possibly due to the low sensitivity of bulk techniques for measuring sublimation – such as thermogravimetric analysis – in comparison to photoemission spectroscopy. In the present measurements, we are only measuring a few nanometers deep into the sample. Thus the spectra shown in Figure 5a represent an extremely slow sublimation rate, that would not be detectible with bulk measurements methods.

Note that the spectra shown in Figure 5a represent a time average (of *ca.* 3 min). There were simultaneous oxidation and sublimation processes occurring on the foil during the acquisition of these spectra. Thus the peak area of the Re_2O_7

species represents the amount of Re_2O_7 present on the surface as a net-result of the simultaneous oxidation and sublimation processes. At 250 °C some Re_2O_7 is still detectible, but at 350 °C and above – i.e. above the literature sublimation temperature of Re_2O_7 – no Re_2O_7 is detectible.

What is especially interesting is that the 'ReO' surface oxide, and also possibly small amounts of Re^{4+} are present on the surface at high temperature. This observation is particularly interesting when one notes that 'ReO' is not a stable bulk oxide. It is only known to exist at the Re-metal surface, however, on the surface it appear to be relatively thermally stable.

The stability of the surface oxide is further examined by the reduction of Re-foil in H_2, as shown in Figure 5b. The Re $4f_{7/2}$ spectra shown here exhibit an Re^{2+} peak from 'ReO', multiple $Re^{\delta+}$ peaks (where $\delta \sim 1$) from O-reconstructed Re, and an Re^0 peak from metallic rhenium. It should be noted that the peak fitting parameters used to fit these spectra – especially the peak parameters used for the $Re^{\delta+}$ species – are based on values determined from previous work on O-reconstructed rhenium single crystals, [13, 39, 40] as mentioned in the discussion of Figure 1b.

In Figure 5b, one can see that as the temperature increases, the Re^{2+} peak diminishes and eventually disappears at $T > 337$ °C. The $Re^{\delta+}$ peaks also diminish with increasing temperature, where the higher-binding-energy peaks diminish at lower temperature than the low-binding-energy peaks. Even at 450 °C, in an atmosphere of 0.3 mbar H_2, some $Re^{\delta+}$ remains. This result suggests that oxygen bound to metallic rhenium – especially the singly-coordinated O-Re bond – is resistant to reduction by H_2 even at elevated temperatures.

In Figure 5b one can also see an apparent shift of the peak maximum for the metallic rhenium peak. At higher temperature, the peak maximum appears at 0.075 eV higher binding energy. We have accounted for this observation by considering the surface core-level shift (SCLS) of surface rhenium atoms. At higher temperatures, the number of surface rhenium atoms that are not coordinated with oxygen increases. This gives rise to bare metal atoms at the surface, and these atoms exhibit slightly different binding energies from the bulk. The SCLS for Re has been examined previously on several accounts. It has been shown that on Re(0001) surfaces, the Re $4f$ peak shift by *ca.* −0.1 eV (i.e. towards lower binding energy compared to the bulk peak). [38, 41, 54] Whereas on the much rougher, faceted Re(12-31) surface, the binding energy shift of surface atoms is in the opposite direction, +0.13 eV. [13, 39, 55] The positive SCLS of Re(12-31) has been previously attributed to a contracted bond length of the highly under-coordinated Re atoms at the Re(12-31) surface. In the present results, we observe a shift towards higher binding energy relative to the bulk, which suggests that the metal's surface is faceted and rough, similar to the observations of the Re(12-31) orientation. [40]

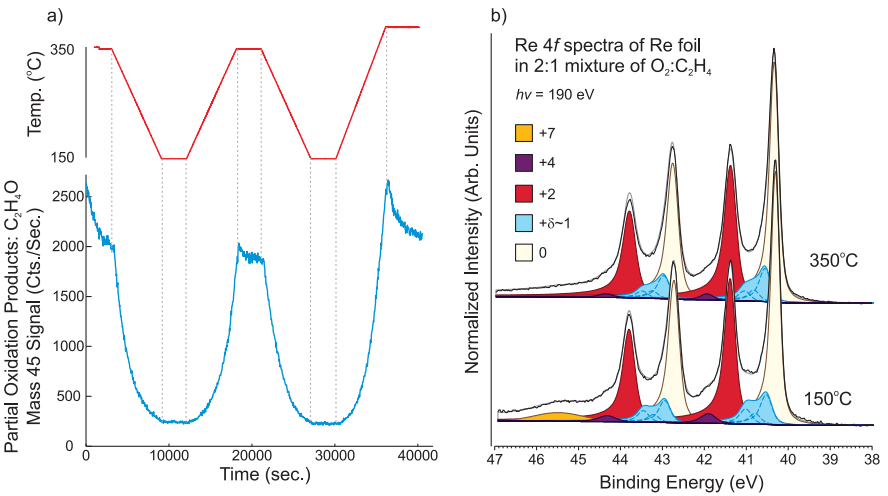

Figure 6: (a) Temperature profile and partial-oxidation product formation (with chemical formula C_2H_4O, measured by PTRMS – i.e. ethene oxide and acetaldehyde) of a rhenium foil subjected to several temperature ramps in a mixture of 2 : 1, O_2 : C_2H_4 (total pressure = 0.3 mbar). (b) Re 4f spectra and corresponding peak fits of the rhenium foil during the temperature ramps described in (a). The top spectrum was measured at 350 °C, when the foil was catalytically active. The bottom spectrum was measured at 150 °C, when the foil was inactive. Rhenium oxidation states are indicated by the legend.

3.4 Active catalyst

In order to investigate the surface species present under catalytic operating conditions, we examined rhenium foil during partial oxidation of ethylene. We performed a series of temperature ramps, cycling between 150 °C and 350 °C, on a rhenium foil sample in an atmosphere consisting of a mixture of O_2 and C_2H_4 (total pressure 0.3 mbar). We monitored the production of partial-oxidation products C_2H_4O (i.e. ethylene epoxide + ethyl aldehyde), using proton-transfer mass spectrometry (by monitoring the mass 45 ion, as described in the experimental section).

Figure 6a shows a series of temperature ramps and partial-oxidation production for rhenium foil in a 2 : 1 mixture of O_2 : C_2H_4. The production of partial-oxidation products indicates the catalyst is active at 350 °C and inactive at 150 °C. During the temperature ramps, we simultaneously measure photoemission spectra, in order to monitor the surface composition of the catalyst in its active and inactive state. We measured Re 4f, O 1s and C 1s spectra. The O 1s spectra did not yield useful information, as the O 1s binding energy of rhenium-oxides proved to be relatively insensitive to rhenium oxidation state. The C 1s spectra exhib-

ited no carbon on the surface. The most informative spectra were from the Re 4*f* region.

The Re 4*f* photoemission spectra of the foil in an active and inactive state are shown in Figure 6b. Here one can see that, for both active and inactive states, a 'ReO' surface oxide and small amounts of Re^{4+} species are present in (as well as several buried $Re^{\delta+}$ species and the Re bulk metal). The main difference between the spectrum from the active catalyst (spectrum at 350 °C) and that of the inactive catalyst (spectrum at 150 °C) is the presence of a small amount of Re_2O_7 on the inactive catalyst. There is also a slight difference in the amount of Re^{4+} species, with a lower amount apparent on the active catalyst.

These observations suggest that at low temperature a thin film of Re_2O_7 forms on the catalyst surface. We tentatively propose that the Re^{4+} and Re^{2+} species may be responsible for the catalytic activity and that the Re_2O_7 layer actually inhibits the reaction. Based on the measured peak intensity of the Re^{7+} species, the Re_2O_7 film that is present at 150 °C is of sub-monolayer coverage, suggesting that perhaps it nucleates at the Re^{4+} defect sites. The hypothesis that Re_2O_7 deactivates the surface is reasonable given that the Re_2O_7 surface consists of high strength terminal Re=O bonds. [1, 56] In fact, previous work on oxides with similar surface terminations have shown such bonding to be chemically inactive. For instance, it was shown that the vanadyl group (V=O) – that terminates the V_2O_5(001) surface and the V_2O_3(0001) surface in oxidizing conditions – does not react with H_2 or methanol unless the oxygen vacancies are created by removal of vanadyl groups. [57–59] Further studies are under way to more closely investigate the active rhenium species during oxidation reactions.

4 Conclusion

By using NAP-XPS to measure rhenium foils under various atmospheric conditions, we find that in an oxidizing environment of $O_2 + 1\%O_3$ (0.3 mbar) a thin film of *ca.* 0.5 nm Re_2O_7 grows on the rhenium foil surface. Buried between the Re_2O_7 film and the metal substrate, we detect a layer of Re^{2+} species, with a small amount of Re^{4+} and $Re^{\delta+}$ species. The Re^{4+} species were attributed to oxidation-state defects caused by either interfacial O-vacancy defects or by spontaneous disproportionation of Re^{2+} at the metal interface. While heating the oxide film in the same oxidizing conditions, we found that the Re_2O_7 layer begins to sublime at *ca.* 150 °C and is completely absent at temperatures greater than 300 °C, While the Re^{4+}, Re^{2+} and $Re^{\delta+}$ species remain on the surface even at temperatures as high as 450 °C. In a reducing environment, Re^{4+} species are not detected, while the Re^{2+}

species remain on the foil surface up to temperatures of 337 °C, and $Re^{\delta+}$ remain up to 550 °C.

When examining rhenium foil under conditions for partial-oxidation of ethylene (2 : 1 ratio of $O_2 : C_2H_4$), we find that, when the catalyst is active (at a temperature of 350 °C), the surface contains Re^{4+}, Re^{2+}, $Re^{\delta+}$ and Re^0 species, with the $Re^{\delta+}$ and Re^0 species presumably buried under the Re^{4+} and Re^{2+} species. On the inactive catalyst surface (at a temperature of 150 °C), it is found that a submonolayer coverage of Re_2O_7 begins to form. We propose that the drop in activity is caused by the Re_2O_7 blocking the active site of the catalyst.

Acknowledgement: We gratefully acknowledge financial support from the Max-Planck Gesellschaft. We also acknowledge the support of the Helmholtz-Zentrum Berlin, especially the invaluable efforts of Dr. Michael Hävecker and Dr. Raoul Blume.

Received January 6, 2014; accepted February 26, 2014.

References

1. W. H. Davenport, V. Kollonitsch, and C. H. Klein, Ind. Eng. Chem. Fund. **60** (1968) 10.
2. S. M. Augustine, G. N. Alameddin, and W. M. H. Sachtler, J. Catal. **115** (1989) 217.
3. N. Wagstaff and R. Prins, J. Catal. **59** (1979) 434.
4. J. Xiao and R. J. Puddephatt, Coordin. Chem. Rev. **143** (1995) 457.
5. A. R. Margarita and M. M. Khabib, Russ. Chem. Rev. **38** (1969) 944.
6. L. Wang, K. Murata, and M. Inaba, Catal. Today **82** (2003) 99.
7. Y. Shu, R. Ohnishi, and M. Ichikawa, Appl. Catal. A-Gen. **252** (2003) 315.
8. J. Okal, Appl. Catal. A-Gen. **287** (2005) 214.
9. J. C. Mol, Catal. Today **51** (1999) 289.
10. S. Vada, A. Hoff, E. ÅdnaneS, D. Schanke, and A. Holmen, Top Catal. **2** (1995) 155.
11. E. L. Kunkes, D. A. Simonetti, J. A. Dumesic, W. D. Pyrz, L. E. Murillo, J. G. Chen, and D. J. Buttrey, J. Catal. **260** (2008) 164.
12. C. B. Wang, Y. P. Cai, and I. E. Wachs, Langmuir **15** (1999) 1223.
13. A. S. Y. Chan, W. Chen, H. Wang, J. E. Rowe, and T. E. Madey, J. Phys. Chem. B **108** (2004) 14643.
14. Y. Z. Yuan, T. Shido, and Y. Iwasawa, Chem. Commun. **15** (2000) 1421.
15. G. Beamson, A. J. Papworth, C. Philipps, A. M. Smith, and R. Whyman, J. Catal. **278** (2011) 228.
16. N. D. Spencer and G. A. Somorjai, J. Catal. **78** (1982) 142.
17. R. Kojima, H. Enomoto, M. Muhler, and K. Aika, Appl. Catal. A-Gen. **246** (2003) 311.
18. J. C. Dellamorte, J. Lauterbach, and M. A. Barteau, Catal. Today **120** (2007) 182.
19. H. C. Yao and M. Shelef, J. Catal. **44** (1976) 392.

20. E. S. Shpiro, M. A. Ryashentseva, K. M. Minachev, G. V. Antoshin, and V. I. Avaev, J. Catal. **55** (1978) 402.
21. G. Rouschia, Chem. Rev. **74** (1974) 531.
22. P. A. Shcheglov and D. V. Drobot, Russ. J. Phys. Chem. **80** (2006) 1819.
23. A. Cimino, B. A. Deangelis, D. Gazzoli, and M. Valigi, Z. Anorg. Allg. Chem. **460** (1980) 86.
24. H. Oppermann, Z. Anorg. Allg. Chem. **523** (1985) 135.
25. K. G. Bramnik, *Ternary and Quaternary Phases in the Alkali-Earth–Rhenium–Oxygen System*, Universität Darmstadt, 2001.
26. C. Bolivar, H. Charcosset, R. Frety, M. Primet, L. Tournayan, C. Betizeau, G. Leclercq, and R. Maurel, J. Catal. **45** (1976) 163.
27. B. H. Isaacs and E. E. Petersen, J. Catal. **85** (1984) 1.
28. D. J. C. Yates and J. H. Sinfelt, J. Catal. **14** (1969) 182.
29. W. T. Tysoe, F. Zaera, and G. A. Somorjai, Surface Science **200** (1988) 1.
30. F. D. Hardcastle, I. E. Wachs, J. A. Horsley, and G. H. Via, J. Mol. Catal. **46** (1988) 15.
31. J. Okal, W. Tylus, and L. Kepinski, J. Catal. **225** (2004) 498.
32. R. M. Edrevakardjieva and A. A. Andreev, J. Catal. **94** (1985) 97.
33. S. R. Adkins and B. H. Davis, Acs Symposium Series **288** (1985) 57.
34. Y. Z. Yuan and Y. Iwasawa, J. Phys. Chem. B **106** (2002) 4441.
35. J. Okal, L. Kepinski, L. Krajczyk, and W. Tylus, J. Catal. **219** (2003) 362.
36. R. Ducros, M. Alnot, J. J. Ehrhardt, M. Housley, G. Piquard, and A. Cassuto, Surf. Sci. **94** (1980) 154.
37. S. Tatarenko, P. Dolle, R. Morancho, M. Alnot, J. J. Ehrhardt, and R. Ducros, Surf. Sci. **134** (1983) L505.
38. R. Ducros and J. Fusy, J. Electron Spectrosc. **42** (1987) 305.
39. A. S. Y. Chan, G. K. Wertheim, H. Wang, M. D. Ulrich, J. E. Rowe, and T. E. Madey, Phys. Rev. B **72** (2005) 035442.
40. H. Wang, A. S. Y. Chan, W. Chen, P. Kaghazchi, T. Jacob, and T. E. Madey, Acs Nano **1** (2007) 449.
41. E. Miniussi, E. R. Hernandez, M. Pozzo, A. Baraldi, E. Vesselli, G. Comelli, S. Lizzit, and D. Alfe, J. Phys. Chem. C **116** (2012) 23297.
42. H. Bluhm, M. Havecker, Knop-A. Gericke, M. Kiskinova, R. Schlogl, and M. Salmeron, MRS Bull. **32** (2007) 1022.
43. Knop-A. Gericke, E. Kleimenov, M. Havecker, R. Blume, D. Teschner, S. Zafeiratos, R. Schlogl, V. I. Bukhtiyarov, V. V. Kaichev, I. P. Prosvirin, A. I. Nizovskii, H. Bluhm, A. Barinov, P. Dudin, and M. Kiskinova, In: *Advances in Catalysis*, Vol 52., B. C. Gates, H. Knozinger (Eds.) 2009, p. 213.
44. J. L. Campbell and T. Papp, Atom. Data Nucl. Data **77** (2001) 1.
45. J. J. Olivero and R. L. Longbothum, J. Quant. Spectrosc. Ra. **17** (1977) 233.
46. S. Doniach and M. Sunjic, J. Phys. C-Solid State **3** (1970) 285.
47. M. T. Greiner, L. Chai, M. G. Helander, W. M. Tang, and Z. H. Lu, Adv. Funct. Mater. **22** (2012) 4557.
48. M. T. Greiner, L. Chai, M. G. Helander, W.-M. Tang, and Z.-H. Lu, Adv. Funct. Mater. **23** (2013) 215.
49. M. Cohen, J. Electrochem. Soc. **121** (1974) C191.
50. W. E. Boggs and R. H. Kachik, J. Electrochem. Soc. **116** (1969) 424.
51. M. Seo, J. B. Lumsden, and R. W. Staehle, Surf. Sci. **50** (1975) 541.

52. R. M. Cornell and U. Schwertmann, *The Iron Oxides: Structure, Properties, Reactions, Occurences and Uses*, 2nd ed., Wiley-VCH, Weinheim, 2003, p. 505.
53. Inelastic mean-free-paths were calculated using the QUASES-IMFP-TPP2M software, which is based on the work of S. Tanuma, C. J. Powell, and D. R. Penn, Surf. Interf. Anal. **21** (1994 165).
54. N. Martensson, H. B. Saalfeld, H. Kuhlenbeck, and M. Neumann, Phys. Rev. B **39** (1989) 8181.
55. Y. Nie, J. Pan, W. Zheng, J. Zhou, and C. Q. Sun, J. Phys. Chem. C **115** (2011) 7450.
56. I. E. Wachs, In: *Metal Oxides - Chemistry and Applications*, J. L. G. Fierro (Ed.), CRC Press, Boca Raton (2006).
57. D. Göbke, Y. Romanyshyn, S. Guimond, J. M. Sturm, H. Kuhlenbeck, J. Döbler, U. Reinhardt, M. V. Ganduglia-Pirovano, J. Sauer, and H.-J. Freund, Angew. Chem. Int. Edit. **48** (2009) 3695.
58. B. Tepper, B. Richter, A. C. Dupuis, H. Kuhlenbeck, C. Hucho, P. Schilbe, M. A. bin Yarmo, and H. J. Freund, Surf. Sci. **496** (2002) 64.
59. Y. Romanyshyn, S. Guimond, H. Kuhlenbeck, S. Kaya, R. P. Blum, H. Niehus, S. Shaikhutdinov, V. Simic-Milosevic, N. Nilius, H. J. Freund, M. V. Ganduglia-Pirovano, R. Fortrie, J. Döbler, and J. Sauer, Top Catal. **50** (2008) 106.